Hydrologic controls on equilibrium soil depths

L. Nicótina,[1] D. G. Tarboton,[2] T. K. Tesfa,[2] and A. Rinaldo[1]

Received 11 May 2010; revised 12 January 2011; accepted 31 January 2011; published 30 April 2011.

[1] This paper deals with modeling the mutual feedbacks between runoff production and geomorphological processes and attributes that lead to patterns of equilibrium soil depth. Our primary goal is an attempt to describe spatial patterns of soil depth resulting from long-term interactions between hydrologic forcings and soil production, erosion, and sediment transport processes under the framework of landscape dynamic equilibrium. Another goal is to set the premises for exploiting the role of soil depths in shaping the hydrologic response of a catchment. The relevance of the study stems from the massive improvement in hydrologic predictions for ungauged basins that would be achieved by using directly soil depths derived from geomorphic features remotely measured and objectively manipulated. Hydrological processes are here described by explicitly accounting for local soil depths and detailed catchment topography. Geomorphological processes are described by means of well-studied geomorphic transport laws. The modeling approach is applied to the semiarid Dry Creek Experimental Watershed, located near Boise, Idaho. Modeled soil depths are compared with field data obtained from an extensive survey of the catchment. Our results show the ability of the model to describe properly the mean soil depth and the broad features of the distribution of measured data. However, local comparisons show significant scatter whose origins are discussed.

Citation: Nicótina, L., D. G. Tarboton, T. K. Tesfa, and A. Rinaldo (2011), Hydrologic controls on equilibrium soil depths, *Water Resour. Res., 47*, W04517, doi:10.1029/2010WR009538.

1. Introduction

[2] Hydrologic controls strongly influence geomorphological processes determining the runoff that contributes to shape the landscape. The interface for these processes is represented by the so-called critical zone, the thin soil layer where rocks, soil, atmospheric gases, and waters strongly interact (see *Anderson et al.* [2007] for details). Therein, the interplay of sediment transport and landscape evolution processes, including erosion, deposition, and soil production, interests different areas of the Earth sciences, including hydrological and carbon sequestration processes, soil formation, and stream water chemistry [*Yoo et al.*, 2005, 2007]. Geological, biological, and hydrologic controls also interact in the coevolution of the critical zone whose extent also defines the control volume for many hydrological and ecological processes [*Dietrich and Perron*, 2006]. From a hydrologic point of view, the prominent role of spatial patterns of soil depth was identified long ago as one of the controlling factors influencing the water balance [*Hewlett and Hibbert*, 1967]. More recently, soil depths have been argued to drastically impact water residence times and streamflow source areas [*Sayama and McDonnell*, 2009; *Botter et al.*, 2010]. This recent evidence follows the wider reasoning that calls for a tighter link between hydrology and pedology in order to predict catchment-scale water fluxes [*Lin et al.*, 2006; *McDonnell et al.*, 2007].

[3] The description of spatial patterns in hydrology is usually constrained by the availability of field data and by our actual capability of deriving suitable boundary conditions from physically based approaches [*Lin et al.*, 2006]. To that end, this work focuses on modeling runoff production as a function of geomorphology and soil depth and on how hydrologic processes interact with soil production and sediment transport. The sediment balance equations that control relief and soil depth apply to landscape evolution theories that include a natural (i.e., evolutionary) geographic cycle of erosion [*Davis*, 1892; *Rinaldo et al.*, 1995; *Hancock and Skinner*, 2000] as well as dynamic equilibrium theory perturbed by periodic tectonic events [*Gilbert*, 1909; *Hack*, 1960; *Bishop*, 2007].

[4] Long-term evolution of landforms requires numerical studies to validate field observations and theoretical hypotheses, and the formulation of proper geomorphic transport laws (to be tested independently from the models employed) may pose some constraint to the generality of modeling results [*Sharp*, 1982; *Dietrich et al.*, 2003; *Dietrich and Perron*, 2006; *Pelletier and Rasmussen*, 2009]. Among the chief transport laws, soil production is ascribed to abiotic (i.e., freeze-thaw cycles, shear deformation, and dissolution-induced bedrock collapse) and biogenic (i.e., tree throw and burrowing effects of animals and insects) controls [*Dietrich et al.*, 1995; *Heimsath et al.*, 1997; *Gabet et al.*, 2003]. The soil production function has been estimated, e.g., through isotope dating techniques, as exponentially declining with

[1]Laboratory of Ecohydrology, École Polytechnique Fédérale Lausanne, Lausanne, Switzerland.
[2]Civil and Environmental Engineering Department, Utah State University, Logan, Utah, USA.

0043-1397/11/2010WR009538

depth [*Dietrich et al.*, 1995; *Heimsath et al.*, 1997]. Other studies [*Anderson et al.*, 2002; *Saco et al.*, 2006] have recognized, however, that soil water content is a driver for several soil production processes either directly (through freeze-thaw cycles or enhancement of chemical weathering) or indirectly (by allowing vegetation to grow and contribute to physical and chemical bedrock weathering). In particular, *Saco et al.* [2006] observed that if the soil production function is not spatially variable, the patterns of soil depth simply reflect erosion rates, implying, under the assumption of dynamic equilibrium, spatial uniformity of the resulting soil depths, a clearly unrealistic case. Recent studies have also modeled soil thickness via different techniques that link it to other topographic and climatic variables (e.g., slope, distance from hilltop, or total contributing area) [*Catani et al.*, 2010]. In this paper we capitalize on such work to attempt a study of the feedbacks between hydrological and soil production processes. To do so, we develop modeling tools that aim at studying equilibrium patterns of soil depth determined by characteristic hydrologic forcings via an iterative procedure. The availability of a comprehensive soil depth data set from our case study also allows direct comparison of model results with field data.

[5] This paper is organized as follows: section 2 describes the study catchment and the field data sets employed, and section 3 discusses the working hypotheses. Results and discussion in sections 4 and 5 conclude the paper, detailing our findings and our interpretations.

2. Study Catchment

[6] The Dry Creek Experimental Watershed (DCEW) is located in the semiarid southwestern region of Idaho, 16 km northeast of the city of Boise, Idaho (Figure 1a). The surrounding area is defined as the Boise Front and includes mountainous and foothills topography. The experimental watershed is delineated as the 28 km^2 northeastward trending Dry Creek drainage from the 1000 m elevation at the junction of Dry Creek with Bogus Basin Road to the headwaters of Dry Creek near Bogus Basin. The headwaters of Dry Creek are located at an elevation of 2100 m in the granitic region of the Boise Front. The perennial creek flows south to southwest from its origin to its confluence with the Boise River west of the city of Boise. Shingle Creek is the only perennial tributary draining into Dry Creek. Numerous unnamed intermittent tributaries flow into Dry Creek within and beyond the DCEW boundary [*Williams*, 2005].

[7] Precipitation peaks occur in winter and spring, and approximately half of the annual precipitation falls as snow; summers are hot and dry, but a persistent snowpack exists from around early November through to March or April (see Figure 2). Streamflow is typically very low, with peaks happening in spring during the snowmelt season (Figure 3). Soils are formed from weathering of the underlying Idaho Batholith, which is a granite intrusion ranging in age from 75 to 85 Ma [*McNamara et al.*, 2005; *Stratton et al.*, 2009]. Soil textures ranges from loam to sandy loam, with south facing slopes showing generally a coarser texture than those on north facing slopes. South facing slopes also have more rock outcrops than the north facing slopes [*Tesfa et al.*, 2009].

[8] The soil depth data used in this work derive from an extensive field campaign carried out by *Tesfa et al.* [2009]. The data set consists of 819 local soil depth measurements clustered into eight subwatersheds and 130 measurements distributed broadly across the watershed (Figure 1b). At

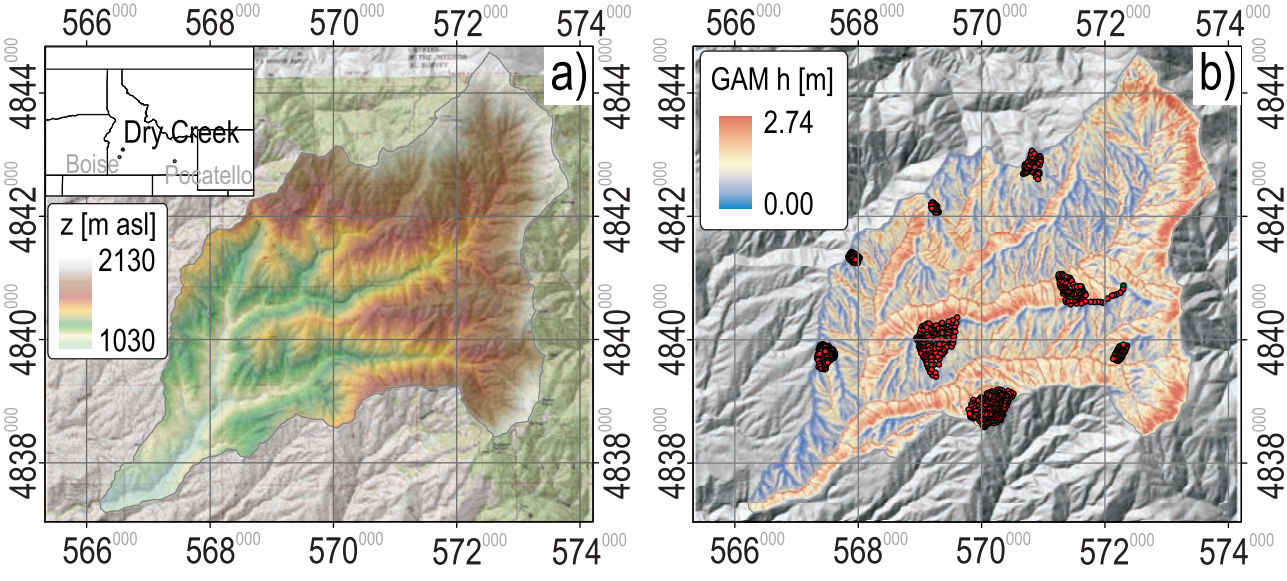

Figure 1. (a) A 1 m lidar digital elevation model (DEM) of the Dry Creek Experimental Watershed (28 km^2). The inset shows the location of the watershed in southwestern Idaho. (b) Soil depth map resulting from the correlation between measured soil depth and several topographic and land cover attributes carried out in a study by *Tesfa et al.* [2009]. The red points indicate the location of the 819 soil depth measurements clustered in distinct watersheds representative of the topography and used in calibration of the model. The statistical model by *Tesfa et al.* [2009] was validated using 130 test locations (not shown) more evenly distributed over the watershed.

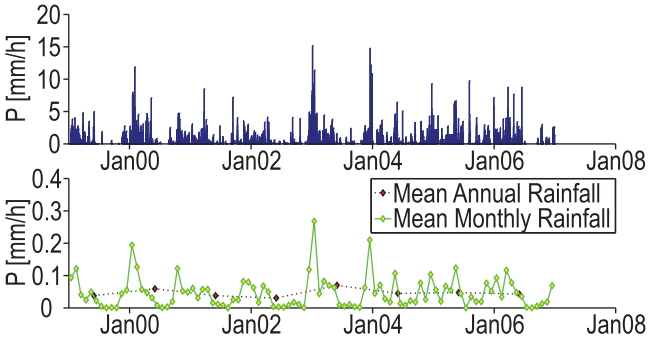

Figure 2. (top) Rainfall data measured at the Lower Weather station in Dry Creek watershed. (bottom) The mean annual and mean monthly precipitation.

each location, two or three soil depth replicates 2–3 m apart were collected by driving a 220 cm long, 1.27 cm diameter sharpened copper-coated steel rod graduated at 5 cm interval vertically into the ground using a fence post pounder until refusal. This method, despite the possibility of underestimating actual soil depth due to the uncertainty to what actually causes the refusal, was the only method feasible given the amount of data collected. As a validation of the method, some measures were carried out in locations close to exposed soil profiles, confirming the depth to bedrock measured with the rod [*Tesfa et al.*, 2009]. *Tesfa et al.* [2009] also explored the correlation between soil depth and different topographic and land cover attributes, proposing a statistical model of soil depths based on the correlation with these variables. Our model results will be compared against their local measures as well as the outcome of the statistical model (Figure 1b) that exhibits a Nash-Sutcliff validation efficiency of 0.47 [*Tesfa et al.*, 2009]. Available data also included 9 year hourly rainfall and runoff time series (1999–2007) as well as a detailed (1 m × 1 m pixel size) digital elevation model (DEM) obtained from a lidar survey of the study catchment. For actual computations described in section 3 the spatial resolution of the grid has been upscaled to 10 m to allow for tractable manipulation of the data.

3. Methods

[9] Soil depth dynamics is controlled by the interactions of land surface and bedrock processes. Topography and hydrology control erosional and depositional processes that determine the conditions for the weathering of the underlying bedrock. The actual depth to bedrock results from a dynamic balance between soil production (the rate of bedrock conversion into soil) and removal by diffusive (topographically driven) or advective (hydrologically driven) sediment transport processes. The hydrologic model adopted herein is based on a spatially distributed representation of soil depths, and this link represents the core of this work, deriving patterns of soil depth at equilibrium and the corresponding hydrologic state of the catchment by means of an iterative procedure.

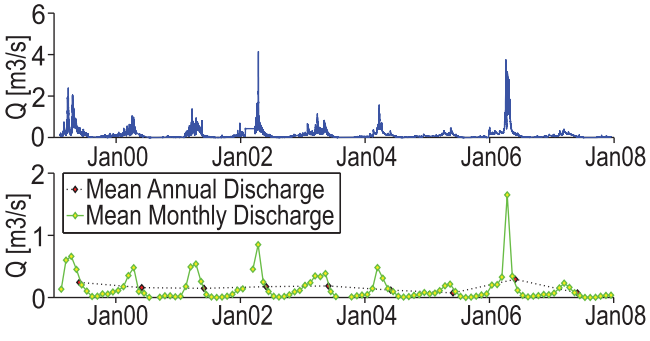

Figure 3. (top) Discharge data measured at the Lower Gage station in Dry Creek watershed. (bottom) The mean annual and mean monthly discharge.

[10] In the presence of a mantled soil layer underlined by bedrock (Figure 4) the regolith mass balance equation can be written as [e.g., *Heimsath et al.*, 1997]

$$\rho_s \frac{\partial h}{\partial t} = -\rho_b \frac{\partial z_b}{\partial t} - \rho_s \vec{\nabla} \cdot \vec{q}_s, \tag{1}$$

where ρ_s and ρ_b are the bulk densities for soil and bedrock, respectively, h is soil depth considered along the vertical direction, z_b is the elevation of the soil-bedrock interface, and $\vec{q}_s$ is sediment flux. In the following, the ratio of soil to bedrock bulk densities will be considered to be approximately 1, thus neglecting ρ_s and ρ_b in applying equation (1). The time evolution of surface elevations $z(t) = z_b(t) + h(t)$ is described through a dynamic balance between the bedrock tectonic uplift rate U and the divergence of the net erosion rate $\vec{q}_s$, quite naturally aligned along topographic gradients:

$$\frac{\partial z}{\partial t} = U - \vec{\nabla} \cdot \vec{q}_s. \tag{2}$$

[11] The landscape is at dynamic equilibrium when the rate of uplift equals the erosion rate and a steady state for elevation is reached $(\partial z/\partial t = 0)$. A state of dynamic equilibrium for the soil layer (characterized by time scales significantly shorter than those attainable for landscape elevations) is reached when the local soil depth does not change in time, with soil production from bedrock being balanced by denudation processes $(\partial h/\partial t = 0)$. Under the hypothesis of soil dynamic equilibrium, we quantify the terms in equation (1) and derive spatial patterns of soil depth which are used, iteratively until convergence, as boundary conditions for the hydrologic model under characteristic meteorological forcings to derive the runoff terms that determine soil erosion.

[12] The first term on the right-hand side of equation (1) represents the local soil production rate, which has been studied and validated through modeling and field experiments based on isotopes dating techniques [*Heimsath et al.*, 1997, 1999; *Gabet et al.*, 2003]. *Heimsath et al.* [1997] showed that an exponential form describes reasonably well the dependence of soil production from soil depth as

$$\frac{\partial z_b}{\partial t} = -p_0 e^{-\gamma h}, \tag{3}$$

where $z_b(t)$ is the elevation of the soil-bedrock interface. Its change over time is always positive and represents the rate of bedrock degradation by biogenic or physical effects.

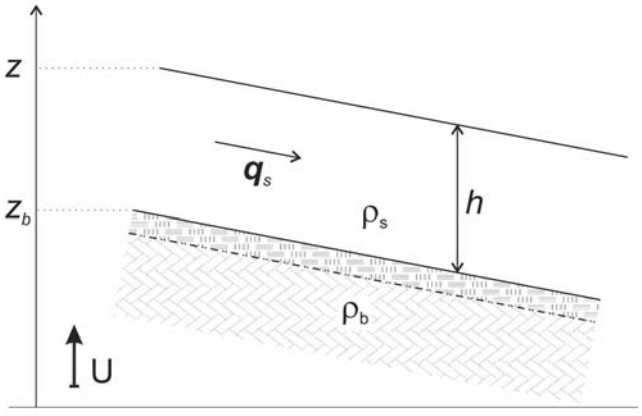

Figure 4. Schematic diagram of hillslope processes.

Here p_0 is a constant rate that defines soil production for exposed bedrock, and γ is the rate of the exponential decay with depth. Here soil depth is used as a proxy for a number of processes that actually take place, inducing mechanical or chemical bedrock disruption and its conversion into soil. Other formulations exist that describe these processes [*Cox*, 1980; *Anderson*, 2002] or hypothesize more elaborate interrelations [e.g., *Saco et al.*, 2006]. Nevertheless, our specific choice is motivated by the fact that soil depth is recognized to exert a first-order control on soil production, as confirmed by the wide use and the noteworthy experimental validation of equation (3) [*Fernandes and Dietrich*, 1997; *Heimsath et al.*, 1997, 1999; *Dietrich and Perron*, 2006; *DiBiase et al.*, 2010].

[13] The erosive term on the right-hand side of equation (1) encompasses diffusive mass wasting and advective, runoff-driven sediment wash and is typically composed of two contributions [*Willgoose et al.*, 1991; *Whipple and Tucker*, 1999]:

$$\vec{q}_s = \vec{q}_{sd}(\nabla z) + \vec{q}_{sa}(R_s, \nabla z), \tag{4}$$

where $\vec{q}_{sd}$ is a diffusive transport flux (dominant in convex hillslopes) directed along steepest descent and proportional to the modulus of the gradient ($\nabla z = |\vec{\nabla} z|$) and $\vec{q}_{sa}$ represents advective transport (dominant in convergent topography), which is a function of runoff R_s and local slope. This latter term encompasses sediment transport processes through rivers, gullies, rills, and sheet overland flow.

[14] The first term in equation (4), comprising diffusive processes such as hillslope soil creep, is modeled as a linear slope-dependent process which when substituted in equation (1) results in [*Gilbert*, 1909; *Culling*, 1963; *Dietrich et al.*, 1995; *Arrowsmith et al.*, 1996; *Fernandes and Dietrich*, 1997; *Furbish and Fagherazzi*, 2001]

$$\vec{\nabla} \cdot \vec{q}_{sd} = \vec{\nabla} \cdot (-K_d \vec{\nabla} z) = -K_d \nabla^2 \mathbf{z}, \tag{5}$$

where K_d is an effective diffusion coefficient and $\nabla^2\mathbf{z}$ is the local (scalar) curvature of the topographic surface. Local curvature is given by the Laplacian of the elevation field (Figure 5) and is evaluated here by a five-point stencil approximation.

[15] It is important to recall that by considering the effect of linear and nonlinear slope-dependent mass wasting on hillslopes, *Roering et al.* [1999] demonstrated that linear diffusive processes asymptotically result in a constant curvature profile along the hillslope, while variable curvature profiles originate from nonlinear mass-wasting processes. This result occurs because low-gradient terrains tend to be highly convex, whereas steep ones approach flat configurations. In fact, for the portion of the catchment where diffusive sediment transport is the dominant soil removal term,

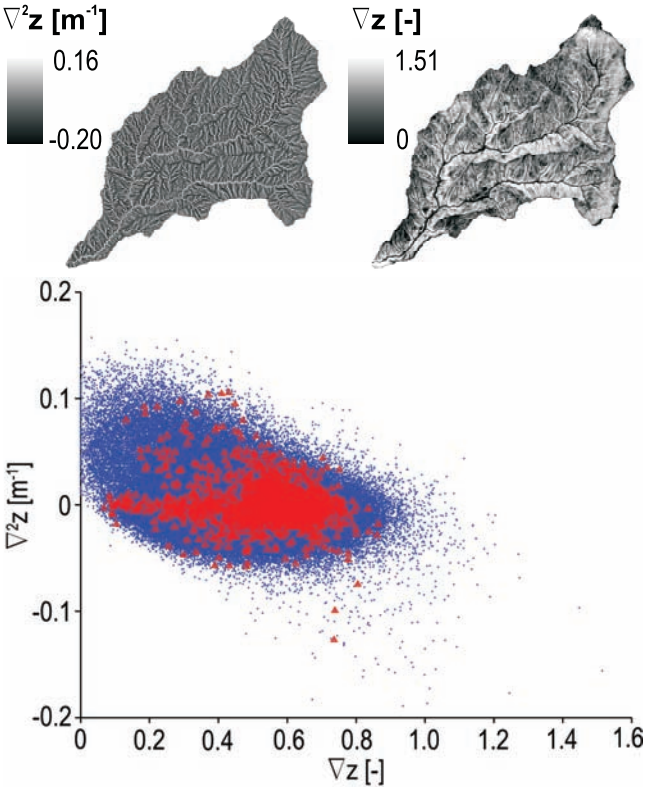

Figure 5. (top) Patterns of slope and curvature determined from the DEM. (bottom) The relation between slope and curvature for convex sites. The triangles represent a single upslope catchment of Dry Creek Experimental Watershed.

substituting equation (5) into (2) under the hypothesis of landscape dynamic equilibrium ($dz/dt \approx 0$) yields

$$\nabla^2 z \approx -\frac{U}{K_d} \tag{6}$$

[16] Figure 5 (bottom) shows the slope-curvature relationships for the DCEW. The color-coded relationship relative to a small first-order subbasin shows that in the range of negative curvatures the curvature remains approximately constant for the whole range of slopes. This supports the choice of a linear model for diffusive transport processes in the case study at hand.

[17] The formulation adopted for modeling geomorphic processes reflects the characteristics of the study catchment. However, it should be noted that the general framework proposed does not depend on the specific processes described, which can be adapted to the problem at hand (e.g., alternative formulations for the soil production function in cases where depth-dependent creep or shallow landsliding are major land-forming agents.)

[18] The advective sediment transport term is tightly related to the stochasticity of the input rainfall signal and provides, in the present framework, the linkage between hydrology and equations of landscape evolution through the iterative procedure described in detail below. Simplistic representations of channel- or overland flow–related transport do not allow us to account for the feedbacks between soil depth patterns and hydrology. Here we adopt a representation that depends on both discharge and slope in the steepest downslope direction [*Smith and Bretherton*, 1972; *Tarboton et al.*, 1992; *Rodriguez-Iturbe and Rinaldo*, 1997; *Istanbulluoglu et al.*, 2003]:

$$\vec{\nabla} \cdot \vec{q}_{sa} \sim \vec{\nabla} \cdot \left[\beta R_s^m (\nabla z)^n \vec{u}\right], \tag{7}$$

where β is a rate parameter for sediment transport, R_s is surface runoff per unit width, ∇z is the local slope magnitude, $\vec{u} = -\vec{\nabla} z/|\vec{\nabla} z|$ is a unit vector in the steepest downslope direction (slope directions are computed with the D-infinity flow model [*Tarboton*, 1997]), and m and n are model parameters. *Banavar et al.* [2001] have shown that reparametrization invariance properties of the small-gradient approximation of the landscape evolution equation prescribes exactly $m/n = 1/2$. However, the values of β, m, and n may be allowed to vary on channels and hillslopes, allowing the representation of different transport processes at different spatial scales (i.e., rain splash, surface wash, or river flow) [*Kirkby*, 1971; *Willgoose et al.*, 1991; *Istanbulluoglu et al.*, 2003; *Saco et al.*, 2006], especially if one assumes $R_s \propto a$, where a is specific catchment area [*Beven and Kirkby*, 1979], which is customary, although unrealistic at times, in erosion-dominated landscape evolution equations [e.g., *Whipple and Tucker*, 1999; *DiBiase et al.*, 2010].

[19] Here we evaluate the runoff term in equation (7) by means of a spatially distributed hydrologic model that is sensitive to local soil depth and the local soil moisture deficit that is related to topography and the aggregate "dryness" of the watershed quantified in terms of base flow. This model is designed to capture the essence of the soil depth–hydrology interaction in a setting where overland flow is generated by saturation excess and thus determined by antecedent moisture conditions. By assuming a spatially homogeneous drainage rate per unit area r and vertically homogeneous hydraulic conductivity K and using the TOPMODEL steady state approximation [*Beven and Kirkby*, 1979], local moisture deficit to saturation $D(\vec{x})$ is defined on the basis of local soil depth $h(\vec{x})$ and topography (through a topographic wetness index defined as $\lambda = a/\nabla z$):

$$D(\vec{x}) = \max\left\{0,\ \eta\left[h(\vec{x}) - \frac{r}{K}\lambda(\vec{x})\right]\right\}, \tag{8}$$

where η represents soil porosity. The specific catchment area a in the expression of the topographic wetness index is defined as the total contributing area per unit contour length and has units of length [L]. Downslope accumulation of a is computed along the direction of steepest descent and is evaluated by the D-infinity model [*Tarboton*, 1997]. Spatial averages of $D(\vec{x})$ result in a function of soil moisture deficit that in turn depends on static topographic and soil properties (h, K, λ, and η) and the single dynamic variable (r), which is interpreted as the drainage rate that supports base flow. We thus establish a relationship between storage, epitomized by soil moisture deficit, and discharge as soil drainage to the base flow:

$$\overline{D} = \Psi(r). \tag{9}$$

[20] The function $\Psi(r)$ is thus obtained from topography, given the runoff regime of the catchment. This function can be inverted numerically, yielding

$$q_b = r = \Psi^{-1}(\overline{D}), \tag{10}$$

where q_b denotes base flow per unit area. Equation (10) quantifies base flow drainage as a function of spatially averaged soil moisture deficit. $\overline{D}$ represents the state variable when integrating the water balance equation during dry periods, and through its final value it determines the average moisture antecedent to rain events. The antecedent (catchment averaged) moisture condition gives, from equation (10), the drainage rate per unit area r, which in turn allows the computation of the pointwise antecedent soil moisture $D(\vec{x})$ from equation (8).

[21] Given the surface water input $P(\vec{x})$, the local saturation excess runoff per unit width $R_s(\vec{x})$ is calculated as

$$R_s(\vec{x}) = \max\left[P(\vec{x})\mathrm{d}x - D(\vec{x})\mathrm{d}x + \sum_j p(j, \vec{x}) R_s(j);\ 0\right]. \tag{11}$$

[22] In this expression, j indexes all the grid cells immediately upslope of grid cell $\vec{x}$, $p(j, \vec{x})$ is the proportion that drains into $\vec{x}$, and dx is the dimension of the grid cell. This expression thus accounts for run-on of water from upslope and its infiltration up to the amount of the deficit $D(\vec{x})$. This is a recursive expression that was evaluated using the upslope accumulation method described by *Tarboton and Baker* [2008] with the proportions $p(j, \vec{x})$ evaluated from the DEM using the D-infinity flow model [*Tarboton*, 1997]. The surface runoff quantified by equation (11) depends on local soil depth through the local soil moisture deficit $D(\vec{x})$, expressed by equation (8). This term also

appears in equation (7), representing in this framework the link between hydrology and geomorphology. Actual computations involve these three equations and iteratively provide equilibrium soil depth patterns. In the following, we derive the expression for the equilibrium soil depth that results from the sediments balance under the hypothesis of dynamic equilibrium.

[23] The climate forcing is simplified into a representation that uses separate wet pulses and dry periods. During discrete wet pulses, drainage and base flow are neglected, while during the dry periods, there is no surface water input, with changes in soil moisture being modeled due to base flow drainage and evapotranspiration. A general treatment of this approach could conveniently make use of a pulsed stochastic representation of rainfall [e.g., *Rodriguez-Iturbe et al.*, 1999]. To avoid overly complicating the analysis and to retain the focus on the geomorphologic-hydrologic interactions, however, here we represent surface water input as a discrete annual instantaneous pulse with a fixed depth. This is deemed reasonable given the specific hydrologic regime of the semiarid alpine catchment at hand (see Figures 2 and 3), where precipitation occurs mainly as snow in a well-defined wet season (from November to March) and discharge peaks are confined to the snowmelt season (April and May). As such, the annual instantaneous pulse represents the total water input regardless of its actual source (that is, whether from direct rainfall or snowmelt), and the fixed depth is set equal to the mean annual rainfall (which comprises liquid and solid rainfall inputs).

[24] During the dry period between two rainfall pulses the catchment-averaged water balance equation is

$$\frac{\mathrm{d}\overline{D}}{\mathrm{d}t} = q_b + \overline{E} = \Psi^{-1}(\overline{D}) + \overline{E}(\overline{D}), \tag{12}$$

where evapotranspiration fluxes $\overline{E}$ are evaluated as a function of the spatially variable water deficit (thus accounting for topography and soil depth) and then averaged over the watershed to solve the mass balance in equation (12). Potential evapotranspiration is evaluated for the study site by the Priestley-Taylor method [*Priestley and Taylor*, 1972; *Maidment*,1993; *Brutsaert*, 2005]:

$$E_{rc} = \beta \frac{\Delta}{\Delta + \gamma}(R_n - G), \tag{13}$$

where the parameter β is assumed to be equal to 1.26, as suggested by *Maidment* [1993], G represents the ground heat flux and is considered here negligible as compared to the net shortwave radiation R_n, Δ is the gradient of the saturated vapor pressure (kPa $^{\circ}\mathrm{C}^{-1}$), which is a known function of temperature, and γ is the psychrometric constant. The net radiation is evaluated as a function of the number of clear-sky hours given the location of the study site (see *Maidment* [1993] for details). Actual evapotranspiration is obtained from potential evapotranspiration under the constraints exerted by the moisture content of the watershed:

$$E(\vec{x}) = f(\theta) E_{rc}, \tag{14}$$

where $f(\theta)$ represents a moisture extraction function that describes moisture restrictions on water extraction from the soil. This formulation assumes that plants can transpire at their full potential E_{rc} for water contents below saturation $(\theta = 1)$ until a dryness state is reached $(\theta_d \approx 0.65\theta_{\mathrm{FC}})$; below this water content and until a wilting point is reached (θ_{WP}), evapotranspiration will decrease linearly from its potential value to zero [*Dingman*, 1994; *Rodriguez-Iturbe and Porporato*, 2004]. For water contents below wilting point, water is obviously no longer available for plants transpiration. Storm mass balance at the catchment scale can be written as

$$\frac{\mathrm{d}\overline{D}}{\mathrm{d}t} = \overline{R_s} - \overline{P}, \tag{15}$$

where $\overline{D}$ represents catchment-averaged water deficit, $\overline{P}$ is the average precipitation over the watershed, and $\overline{R_s}$ is the catchment-averaged surface runoff expressed on a per unit area basis.

[25] Substitution of equations (3), (5), and (7) into (1) gives the mass balance for the soil depth. Under the hypothesis of soil dynamic equilibrium, this equation can be solved for the soil depth $h_{eq}(\vec{x})$ (i.e., there is no change in soil depth in time as a result of a dynamic balance between soil production from the underlying bedrock and soil removal from erosion):

$$h_{eq}(\vec{x}) = -\frac{1}{\gamma} \log\left[-\frac{K_d \nabla^2 z + \beta\, \vec{\nabla} \cdot (R_s^m\, |\nabla z|^n\, \vec{u})}{p_0} \right], \tag{16}$$

where now $h_{eq}(\vec{x})$ indicates the local equilibrium soil depth resulting from the given topography and hydrologic regime of the catchment. Equation (16) applies to actively eroding regions of the landscape, where soil production resulting from bedrock disruption is balanced by erosive fluxes keeping the soil depth at equilibrium. The surface discharge term R_s in equation (16) connects geomorphology and hydrology since it accounts for the spatial soil depth pattern involved in the generation of runoff. Equation (16) is solved iteratively with an initial condition for the soil depth set to 1 m, providing at each iteration a different boundary condition for the hydrologic model and thus for the evaluation of hydrologic fluxes appearing in the equation itself. Note that the initial condition must not (and does not) have any significant effects on the model results. The details of the computations are as follows:

[26] 1. An initial condition is assumed for the soil layer. From equation (8) the spatially distributed soil moisture deficit is obtained.

[27] 2. Given climatic conditions, the broad features of the hydrologic response in terms of surface runoff and base flow are quantified.

[28] 3. The obtained spatial patterns are used to solve the sediment balance under dynamic equilibrium, deriving the corresponding local soil depth (through equation (16)), which is used to run the hydrologic model again.

[29] 4. We then iterate the second and third steps until convergence.

4. Results

[30] Soil depth is the controlling parameter in the partition of water fluxes in the hydrologic model. Figure 6

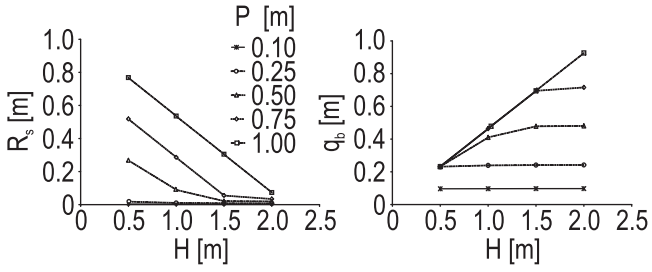

Figure 6. (left) Surface runoff and (right) base flow plotted against spatially homogeneous soil depths. The different curves in the plot refer to different values of spatially homogeneous precipitation depths *P*.

shows the behavior of the model in terms of catchment-averaged fluxes for different spatially homogeneous soil depths and rainfall depths (the other simulation parameters are reported in Table 1). The soil depth, whether spatially homogeneous or variable, controls the partition of the water balance and thus the amount of water available as surface runoff, which in turn controls the potential for sediment transport. The cyclic rainfall assumption discussed in section 3 provides fixed rainfall amounts (constant rainfall depth) at a given interstorm period of 1 year so that stationary hydrologic conditions, relative to the given soil depth pattern, are reached. In each model run the rainfall depth adopted in the scheme is fixed, but it is allowed to vary among runs, with the purpose of analyzing the behavior of the model in response to the climatic forcing (see Figures 6 and 7).

[31] Figure 7 compares model results for two runs. The first run (red dotted line), relative to the soil depth map that fits the field data (Figure 1b) from *Tesfa et al.* [2009], shows that the catchment-averaged surface runoff increases with precipitation, and it is possible to identify a threshold precipitation that distinguishes two different behaviors. (1) The first behavior is water limited, where average surface runoff increases slowly with precipitation and its amount depends on the spatial distribution of the wetness indexes; base flow per unit area shows a nonlinear increase in this region. (2) The second is energy limited, where the subsurface response cannot further increase and excess water

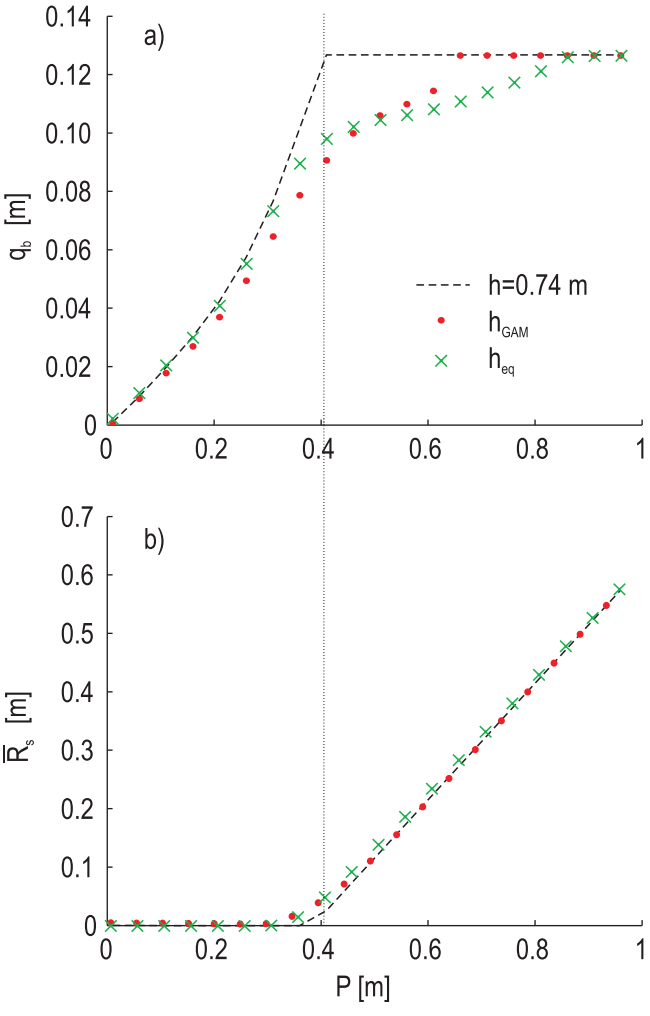

Figure 7. Model response for homogeneous (black dashed line) and spatially variable soil depth patterns (red dots and green crosses) evaluated in terms of (a) steady state baseflow and (b) surface runoff, corresponding to different amount of precipitation. Spatially variable soil depth results are from the best fit of the GAM statistical model obtained by *Tesfa et al.* [2009]. Homogeneous soil depth was set equal to the mean of the GAM soil depth distribution.

Table 1. Model Parameters Adopted for the Simulations Presented in This Study

Model	Parameter[a]	Value	Unit
Hydrology	K_h	10^{-6}	m/s
	η	0.5	
	θ_{WP}	0.05	
	θ_{FC}	0.18	
Landscape evolution	K_d	5×10^{-4}	m^2/yr
	β	10^{-5}	
	m	2.5	
	n	2.1	
	p_0	8×10^{-5}	m/yr
	γ	3.2	1/m

[a]Parameters are as follows: K_h is the hydraulic conductivity of the soil layer; η is porosity; θ_{WP} is the water content at permanent wilting point; θ_{FC} is the water content at field capacity; K_d is soil diffusivity for diffusive sediment transport; β, m, n are rate coefficient and exponents for advective sediment transport; p_0 is the soil production rate for exposed bedrock; and γ is the rate of the exponential soil production decay with depth.

is available as surface runoff, which assumes a constant value after saturation. The dashed line in Figure 7 corresponds to the simulation run with homogeneous soil depth and with the same mean depth as in the GAM soil depth map (other model parameters are constant and reported in Table 1). This curve represents the envelope curve for the transition between water- and energy-limited conditions; a spatially variable soil depth distribution manifests its effects in the transition region (where the average annual precipitation value in the Dry Creek watershed actually lies).

[32] An iterative solution to equation (16) matching the hydrologic and landscape evolution models allows the identification of equilibrium soil depth patterns based on the actual topography and hydrologic regime of the catchment. The pattern of soil depth is obtained by applying equation (16) with standard literature parameters (reported in Table 1) for erosion and soil production processes under the hypothesis of soil dynamic equilibrium (i.e., $dh/dt \sim 0$;

that is, soil production and removal are in dynamic equilibrium). The applied hypotheses only hold in actively eroding landscapes, thus constraining the analysis to this region, as no dynamic equilibrium is attainable in the presence of soil accumulation. The resulting soil depth map for the Dry Creek Experimental Watershed is shown in Figure 8a. The model correctly simulates the maximum depth in the watershed of the order of 2 m. Maximum soil depths occur at the base of hillslopes and on the eastern boundary of the watershed. The comparison with the soil depth map obtained with the statistical GAM model by *Tesfa et al.* [2009] (reported in Figure 1b) confirms the higher soil depths on the eastern boundary of the watershed but also highlights several differences. Figure 8b maps the local difference between the soil depths obtained in this work and the one obtained by *Tesfa et al.* [2009]. In fact, the statistical model reproduces the deeper soil depths observed on north facing slopes, while the physical model developed does not have a mechanism to reproduce this characteristic. It also appears that the physical model generally predicts deeper soil depths compared to the statistical model, e.g., proceeding toward the outlet of the catchment because of the gentler topography in that part of the watershed.

[33] Figure 9 compares the distribution of the modeled soil depths (Figure 9a) with soil depths obtained from the GAM model (Figure 9b). Also, in this case the comparison

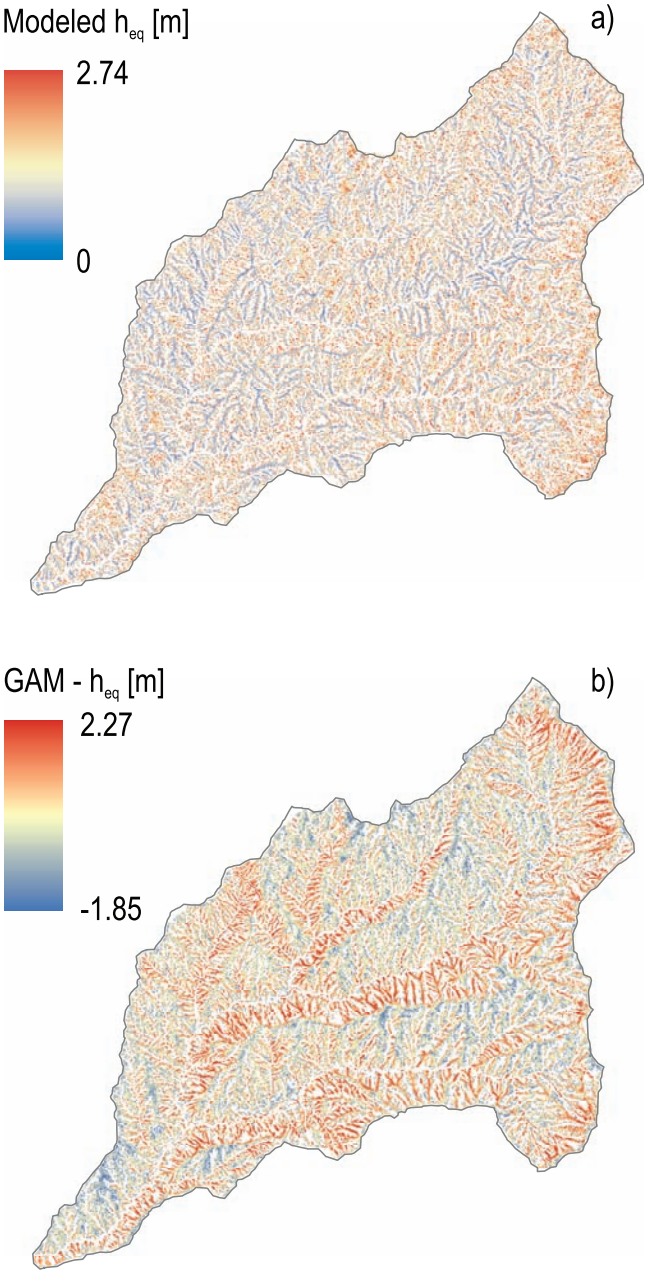

Figure 8. Modeled soil depths and comparison with the statistical reproduction [*Tesfa et al.*, 2009] of soil depth in the study catchment. (a) Soil depth map obtained with the physical model described in this paper. (b) Error map, representing the local absolute difference between the soil depth obtained by the statistical model of *Tesfa et al.* [2009] (GAM) and the equilibrium soil depth predicted with the physical model.

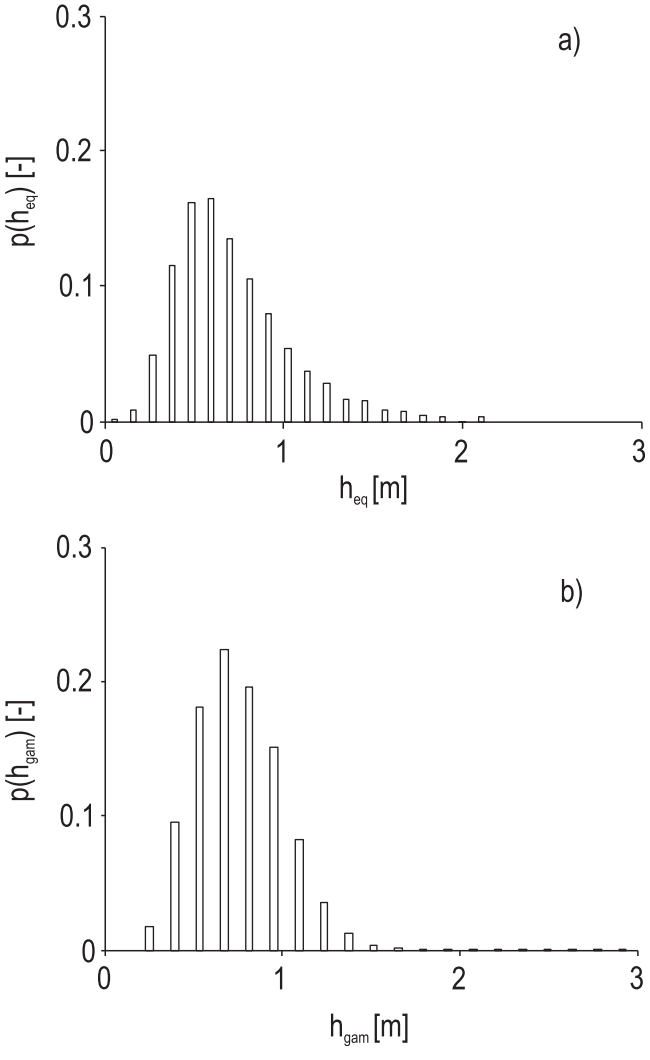

Figure 9. Comparison of (a) the soil depth distribution obtained from the application of the model with (b) that derived from the GAM model [*Tesfa et al.*, 2009]. The comparison refers to actively eroding sites in the study catchment, where local soil depth can be quantified by the proposed model.

is limited to the actively eroding portions of the catchment. We note a satisfactory capability of predicting the range of soil depths. The two distributions have a comparable mean (0.71 m for the physical model and 0.78 m for the GAM model). The soil depths derived from the physical model exhibit a slightly shorter tail. The physical model, however, is capable of predicting rock outcrops that the statistical model cannot predict. The presence of rock outcrops indicates topographic configurations that do not allow us to achieve a dynamic equilibrium soil removal rate that is higher than soil production. However, the topographic setting that induces this condition is identifiable in this framework, which allows us to recognize the location where such a dynamic equilibrium is not attainable.

[34] Figure 10 shows the local comparison of model results with measured soil depths. The comparison was for a subset of 493 of the locations in the available measured data set composed of measurement points located on actively eroding sites (the locations for which meaningful soil depths can be predicted by the model). The dashed line indicates the desired 1:1 line of perfect agreement. Figure 10 presents a significant scatter, and the model does not predict accurately local values of soil depth. The performance of the model is quantified by a Nash-Sutcliff efficiency [*Nash and Sutcliffe*, 1970] of 0.1. This performance appears to be lower than that obtained by *Tesfa et al.* [2009]; however, the lower efficiency is justified by the fact that the physical model does not make use of soil depth information for calibration. The modeled soil depths do not show a constant bias, but it is possible to observe a tendency to underestimate high soil depths. As confirmed by the low value of the Nash-Sutcliff efficiency, the cloud of model values represents well the mean soil depth but does not describe satisfactorily the local values.

[35] The equilibrium soil depth map obtained by the application of the model has also been used to force the hydrologic model. The results, in terms of discharge at the Lower Gage located at the outlet of the DCEW, are plotted in Figure 11. Notwithstanding the schematic character of the hydrologic model at hand as described in section 3 (in particular, on the instantaneous transfer to the outlet of locally produced runoff), Figure 11 shows that the model captures the main functioning of the rainfall-runoff processes in the catchment. In fact, total discharge volumes and their timing are satisfactorily reproduced.

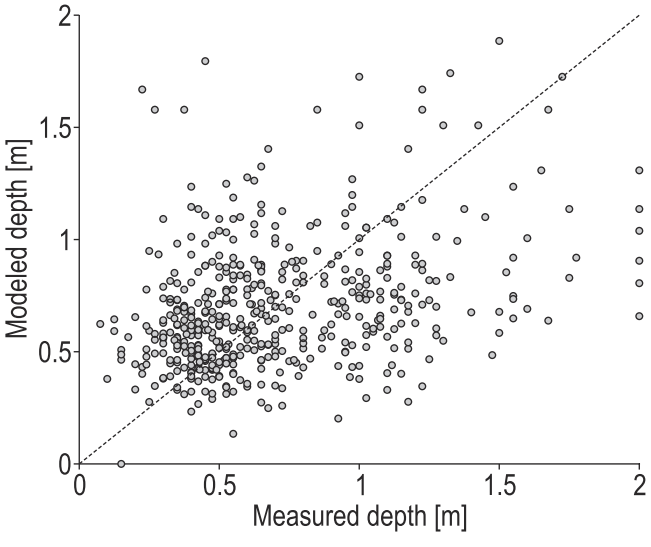

Figure 10. Local comparison of predicted and measured soil depth.

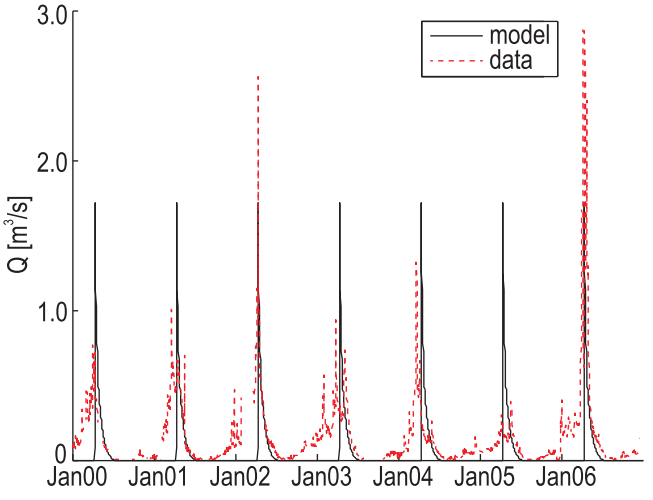

Figure 11. Measured versus computed discharge. The simulation of the hydrologic model was run with the soil depth map obtained through the application of the model.

[36] We believe that the above results represent a significant step forward toward a general theory of the hydrologic response, the poor fit of local soil depths notwithstanding. In fact, on one hand, the model predicts well equilibrium mean soil depths, thus arguably allowing a proper evaluation of catchment-scale water dynamics of runoff production (as shown in Figure 11 and as further work in progress shows). Indeed, the off-line determination of soil depths will allow a next generation of modeling tools for predicting hydrologic response in ungauged basins. On the other hand, it is easy to spot the number of stringent assumptions that may be selectively relaxed while still maintaining the given framework of feedbacks between hydrology, climate, and geomorphology. This obviously may be done for the case study at hand (a semiarid catchment) or any other. Progress may come, for instance, from the use of detrital cosmogenic ^{10}Be, which may allow measures of long-term erosion rates even in catchments characterized by strong relief, precipitation, and lithology gradients, thus allowing us to isolate a much improved relationship between topographic form and erosion rates [*DiBiase et al.*, 2010]. Landscape-forming climatic events have also been crudely modeled in the framework of the proof of concept chosen herein. This can certainly be improved, for instance, by employing a stochastic Poisson point process for daily rainfall arrivals [e.g., *Rodriguez-Iturbe et al.*, 1999] or using a backward framework from measured, variant water residence time distributions [*Botter et al.*, 2010].

5. Conclusions

[37] The geomorphic processes that give rise to actual patterns of soil depth have been studied. In particular, we focused on the interactions between hydrology and geomorphology and their impact on determination of soil

depths. Landscape-forming processes lead, through climatic interactions, to the actual catchment shapes, and soil depth is one of the prominent parameters when dealing with hydrologic modeling for flood forecasting or transport processes at the catchment scale. In fact, the quantification of available subsurface storage is deemed fundamental.

[38] We have proposed a quantitative, pointwise evaluation of soil depths based on topography and on a conceptualized rainfall-runoff scheme whose detailed specification must remain immaterial. The value of these analyses resides in the coupling of well-studied geomorphic transport law with a tailored hydrologic scheme that provides a spatially variable description of the hydrologic balance based on local soil depth. The availability of an extensive survey of soil depths in the study catchment, carried out by one of the authors, allowed direct comparison of model results with field data. The generality of the approach is not affected by the specific choices of transport and soil production models. Different geodynamic settings might be required in other geologic environments where specific processes dominate soil productions and redistributions.

[39] The proposed model results showed the capability of the model to represent the broad characters of actual soil depth distribution. The potential of the coupling between hydrology and geomorphology was limited by the hypothesis of dynamic equilibrium, required for deriving equilibrium soil depth under steady hydrologic conditions. This resulted in equilibrium soil depths obtainable over actively eroding sites only, with the remaining part of the catchment not being at dynamic equilibrium.

[40] The comparison with field data showed a significant scatter between modeled and measured soil depths, characterized by low Nash-Sutcliff efficiency, implying that model results are close to the mean of the observed values but do not pointwise match local soil depth values. We claim, however, that the knowledge of average catchment-scale soil depth values represents a relevant guideline for hydrologic modeling when dealing with lumped or semidistributed models, providing quantitative guidance in the definition of available subsurface storage. Moreover, the model does not require fitting of parameters, whose values were derived from the literature. The proposed model thus represents an effective tool for deriving soil depth information from topography alone. We thus argue that in ungauged catchments our model might, indeed, impact the determination of one of the most uncertain yet fundamental factors, affecting especially runoff partitioning, and the determination of water and solutes residence times.

[41] **Acknowledgments.** The authors would like to thank J. McNamara and his research group for sharing their data for the Dry Creek Experimental Watershed. Funds provided by ERC Advanced grant RINEC 22761 and SFN grant 200021-124930/1 are gratefully acknowledged.

References

Anderson, R. (2002), Modeling the tor-dotted crests, bedrock edges, and parabolic profiles of high alpine surfaces of the Wind River Range, Wyoming, *Geomorphology*, *46*, 35–58, doi:10.1016/S0169-555X(02)00053-3.

Anderson, R., W. Dietrich, and G. Brimhall (2002), Weathering profiles, mass-balance analysis and rates of solute loss: Linkages between weathering and erosion in a small, steep catchment, *Geol. Soc. Am. Bull*, *114*, 1143–1158.

Anderson, S., F. von Blanckenburg, and A. White (2007), Physical and chemical controls on the critical zone, *Elements*, *3*, 315–319, doi:10.2113/gselements.3.5.315.

Arrowsmith, J., D. Pollard, and D. Rhodes (1996), Hillslope development in areas of active tectonics, *J. Geophys. Res.*, *101*, 6255–6275, doi:10.1029/95JB02583.

Banavar, J., F. Calaiori, A. Flammini, A. Maritan, and A. Rinaldo (2001), Scaling, optimality and landscape evolution, *J. Stat. Phys.*, *104*(1-2), 1–48, doi:110.1023/A:1010397325029.

Beven, K., and M. Kirkby (1979), A physically based variable contributing area model of basin hydrology, *Hydrol. Sci. Bull.*, *24*(1), 43–69.

Bishop, P. (2007), Long-term landscape evolution: Linking tectonics and surface processes, *Earth Surf. Processes Landforms*, *32*, 329–365, doi:10.1002/esp.1493.

Botter, G., E. Bertuzzo, and A. Rinaldo (2010), Transport in the hydrologic response: Travel time distributions, soil moisture dynamics, and the old water paradox, *Water Resour. Res.*, *46*, W03514, doi:10.1029/2009WR008371.

Brutsaert, W. (2005), *Hydrology: An Introduction*, Cambridge Univ. Press, New York.

Catani, F., S. Segoni, and G. Falorni (2010), An empirical geomorphology-based approach to the spatial prediction of soil thickness at catchment scale, *Water Resour. Res.*, *46*, W05508, doi:10.1029/2008WR007450.

Cox, N. (1980), On the relationship between bedrock lowering and regolith thickness, *Earth Surf. Processes Landforms*, *5*, 271–274.

Culling, W. (1963), Soil creep and the development of hillside slopes, *J. Geol.*, *71*, 127–161, doi:10.1086/626891.

Davis, W. (1892), The convex profile of badland divides, *Science*, *20*, 245, doi:10.1126/science.ns-20.508.245.

DiBiase, R. A., K. X. Whipple, A. M. Heimsath, and W. B. Ouimet (2010), Landscape form and millennial erosion rates in the San Gabriel Mountains, CA, *Earth Planet. Sci. Lett.*, *289*, 134–144, doi:10.1016/j.epsl.2009.10.036.

Dietrich, W., and J. Perron (2006), The search for a topographic signature of life, *Nature*, *439*, 411–418, doi:10.1038/nature04452.

Dietrich, W., M. Hsu, and D. Montgomery (1995), A process-based model for colluvial soil depth and shallow landsliding using digital elevation data, *Hydrol. Processes*, *9*, 383–400.

Dietrich, W., D. Bellugi, L. Sklar, J. Stock, A. Heimsath, and J. Roering (2003), Geomorphic transport laws for predicting landscape forms and dynamics, in *Prediction in Geomorphology, Geophys. Monogr. Ser.*, vol. 135, pp. 103–132, doi:10.1029/135GM09, AGU, Washington, D. C.

Dingman, S. (1994), *Physical Hydrology*, 575 pp., Macmillian, New York.

Fernandes, N., and W. Dietrich (1997), Hillslope evolution by diffusive processes: The timescale for equilibrium adjustments, *Water Resour. Res.*, *33*, 1307–1318, doi:10.1029/97WR00534.

Furbish, D., and S. Fagherazzi (2001), Stability of creeping soil and implications for hillslope evolution, *Water Resour. Res.*, *37*, 2607–2618, doi:10.1029/2001WR000239.

Gabet, E., O. Reichman, and E. Seabloom (2003), The effects of bioturbation on soil processes and sediment transport, *Annu. Rev. Earth Planet. Sci.*, *31*, 249–273, doi:10.1146/annurev.earth.31.100901.141314.

Gilbert, G. (1909), The convexity of hilltops, *J. Geol.*, *17*, 344–350.

Hack, J. (1960), Interpretations of erosional topography in humid temperate regions, *Am. J. Sci.*, *258-A*, 80–97.

Hancock, P., and B. Skinner (2000), Landscape evolution, in *The Oxford Companion to the Earth*, Oxford Univ. Press.

Heimsath, A., W. Dietrich, K. Nishiizumi, and R. Finkel (1997), The soil production function and landscape equilibrium, *Nature*, *388*, 358–361.

Heimsath, A., W. Dietrich, K. Nishiizumi, and R. Finkel (1999), Cosmogenic nuclides, topography, and the spatial variation of soil depth, *Geomorphology*, *27*, 151–172.

Hewlett, J., and A. Hibbert (1967), Factors affecting the response of small watersheds to precipitation in humid areas, in *International Symposium on Forest Hydrology*, edited by W. Sopper and H. Lull, pp. 275–290, Pergamon, New York.

Istanbulluoglu, E., D. Tarboton, R. Pack, and C. Luce (2003), A sediment transport model for incision of gullies on steep topography, *Water Resour. Res.*, *39*(4), 1103, doi:10.1029/2002WR001467.

Kirkby, M. (1971), Hillslope process-response based on the continuity equation, in *Slope Forms and Processes*, vol. 3, pp. 15–30, Inst. Br. Geogr.

Lin, H., J. Bouma, Y. Pachpsky, A. Western, J. Thompson, R. van Genuchten, H. Vogel, and A. Lilly (2006), Hydropedology: Synergistic integration of pedology and hydrology, *Water Resour. Res.*, *42*, W05301, doi:10.1029/2005WR004085.

Maidment, D. (1993), *Handbook of Hydrology*, McGraw-Hill, New York.
McDonnell, J., et al. (2007), Moving beyond heterogeneity and process complexity: A new vision for watershed hydrology, *Water Resour. Res.*, *43*, W07301, doi:10.1029/2006WR005467.
McNamara, J., C. Chandler, M. Seyfried, and S. Achet (2005), Soil moisture states, lateral flow, and streamflow generation in a semi-arid, snowmelt-driven catchment, *Hydrol. Processes*, *19*, 4023–4038, doi:10.1002/hyp.5869.
Nash, J., and J. Sutcliffe (1970), River flow forecasting through conceptual models, Part I—A discussion of principles, *J. Hydrol.*, *10*(3), 282–290, doi:10.1016/0022-1694(70)90255-6.
Pelletier, J., and C. Rasmussen (2009), Geomorphically based predictive mapping of soil thickness in upland watersheds, *Water Resour. Res.*, *45*, W09417, doi:10.1029/2008WR007319.
Priestley, C., and R. Taylor (1972), On the assessment of surface heat flux and evaporation using large scale parameters, *Mon. Weather Rev.*, *100*, 81–92.
Rinaldo, A., W. Dietrich, G. Vogel, R. Rigon, and I. Rodriguez-Iturbe (1995), Geomorphological signatures of varying climate, *Nature*, *374*, 632–636.
Rodriguez-Iturbe, I., and A. Porporato (2004), *Ecohydrology of Water-Controlled Ecosystems*, Cambridge Univ. Press, New York.
Rodriguez-Iturbe, I., and A. Rinaldo (1997), *Fractal River Basins: Chance and Self-Organization*, 564 pp., Cambridge Univ. Press, New York.
Rodriguez-Iturbe, I., A. Porporato, L. Ridolfi, V. Isham, and D. Cox (1999), Probabilistic modelling of water balance at a point: The role of climate soil and vegetation, *Proc. R. Soc. London, Ser. A*, *455*, 3789–3805.
Roering, J., J. Kirchner, and W. Dietrich (1999), Evidence for nonlinear, diffusive sediment transport on hillslopes and implications for landscape morphology, *Water Resour. Res.*, *35*(3), 853–870, doi:10.1029/1998WR900090.
Saco, P., G. Willgoose, and G. Hancock (2006), Spatial organization of soil depths using a landform evolution model, *J. Geophys. Res.*, *111*, F02016, doi:10.1029/2005JF000351.
Sayama, T., and J. McDonnell (2009), A new time-space accounting scheme to predict stream water residence time and hydrograph source components at the watershed scale, *Water Resour. Res.*, *45*, W07401, doi:10.1029/2008WR007549.
Sharp, R. (1982), Landscape evolution (a review), *Proc. Natl. Acad. Sci. U. S. A.*, *79*, 4477–4486.
Smith, T., and F. Bretherton (1972), Stability and the conservation of mass in drainage basin evolution, *Water Resour. Res.*, *8*, 1506–1529, doi:10.1029/WR008i006p01506.
Stratton, B., V. Sridhar, M. Gribb, J. McNamara, and B. Narasimhan (2009), Modeling the spatially varying water balance processes in a semiarid mountainous watershed of Idaho, *J. Am. Water Resour. Assoc.*, *45*, 1390–1408, doi:10.1111/j.1752-1688.2009.00371.x.
Tarboton, D. (1997), A new method for the determination of flow directions and upslope areas in grid digital elevation models, *Water Resour. Res.*, *33*, 309–320, doi:10.1029/96WR03137.
Tarboton, D., and M. Baker (2008), Towards an algebra for terrain-based flow analysis, in *Representing, Modeling and Visualizing the Natural Environment: Innovations in GIS 13*, edited by N. Mount et al., pp. 167–195, CRC Press, Boca Raton, Fla.
Tarboton, D., R. Bras, and I. Rodriguez-Iturbe (1992), A physical basis for drainage density, *Geomorphology*, *5*, 59–76.
Tesfa, T., D. Tarboton, D. Chandler, and J. McNamara (2009), Modeling soil depth from topographic and land cover attributes, *Water Resour. Res.*, *45*, W10438, doi:10.1029/2008WR007474.
Whipple, K., and G. Tucker (1999), Dynamics of the stream-power river incision model: Implications for height limits of mountain ranges, landscape response timescales, and research needs, *J. Geophys. Res.*, *104*, 17,661–17,674, doi:10.1029/1999JB900120.
Willgoose, G., R. Bras, and I. Rodriguez-Iturbe (1991), A coupled channel network growth and hillslope evolution model: 1. Theory, *Water Resour. Res.*, *27*(7), 1671–1684, doi:10.1029/91WR00935.
Williams, C. (2005), Characterization of the spatial and temporal controls on soil moisture and streamflow generation in a semi-arid headwater catchment, Ph.D. thesis, Boise State Univ., Boise, Idaho.
Yoo, K., R. Amundson, A. Heimsath, and W. Dietrich (2005), Erosion of upland hillslope soil organic carbon: Coupling field measurements with a sediment transport model, *Global Biogeochem. Cycles*, *19*, GB3003, doi:10.1029/2004GB002271.
Yoo, K., R. Amundson, A. Heimsath, W. Dietrich, and G. Brimhall (2007), Integration of geochemical mass balance with sediment transport to calculate rates of soil chemical weathering and transport on hillslopes, *J. Geophys. Res.*, *112*, F02013, doi:10.1029/2005JF000402.

L. Nicótina and A. Rinaldo, Laboratory of Echohydrology, École Polytechnique Fédérale Lausanne, GR C1 565, Station 2, CH-1015, Lausanne, Switzerland. (ludovico.nicotina@epfl.ch; andrea.rinaldo@epfl.ch)

D. G. Tarboton and T. K. Tesfa, Civil and Environmental Engineering Department, Utah State University, 4110 Old Main Hill, Logan, UT 84322, USA. (david.tarboton@usu.edu; t.k.t.@aggiemail.usu.edu)